RESEARCH ARTICLE | NOVEMBER 20 2023

Peculiarities of aerodynamic loads on a projectile in transonic flight at small angles of attack

A. Kuzmin ✉; K. Babarykin

AIP Conf. Proc. 2953, 060005 (2023)
https://doi.org/10.1063/5.0177488

Peculiarities of Aerodynamic Loads on a Projectile in Transonic Flight at Small Angles of Attack

A. Kuzmin[1,a)] and K. Babarykin[1,b)]

[1]*St. Petersburg State University, 28 University Ave, St. Petersburg, 198504 Russia*

[a)] Corresponding author: a.kuzmin@spbu.ru
[b)] konst20@mail.ru

Abstract. Numerical simulations of 3D turbulent flow over a projectile model have been performed at the angles of attack $\alpha = 4°$ and $\alpha = 6°$ at high subsonic free-stream Mach numbers M_∞. The simulations are based on the unsteady Reynolds-averaged Navier-Stokes equations using the k-ω Shear Stress Transport and Detached Eddy Simulation turbulence models. The obtained solutions reveal an intricate behavior of the lift force and pitching moment as functions of M_∞. Locations of shock waves and supersonic regions on the projectile are discussed, and a physical interpretation of two discontinuities in the dependence of aerodynamic coefficients on M_∞ is suggested.

INTRODUCTION

It was established in ballistic and wind-tunnel measurements of 1980s that aerodynamic characteristics of boat-tail projectiles change intricately at high subsonic speeds of flight. In particular, with increasing free-stream Mach number M_∞ at a positive angle of attack, the normal aerodynamic force drops rapidly to a so-called critical point, then rises sharply to another critical point, and after that it drops once again. The intricate behavior of aerodynamic loads must be obviously taken into account in numerical predictions of the trajectory and stability of flight.

In 1990s, Sahu and Nietubic [1] performed numerical simulations of 3D turbulent flow over several projectiles using a k-ε and algebraic eddy viscosity turbulence models. The calculated normal force and pitching moment were in a good agreement with experimental data. Then, Budge [2] carried out computations of 3D flow over two projectiles using a finite-difference solver and Baldwin-Barth turbulence model. He studied flow evolution at the angle of attack of 4° and confirmed the "transonic critical behavior" of the pitching moment and normal force with increasing M_∞. Shock wave locations were shown to influence the pressure distribution over the projectile and cause a decrease in the normal force before the first critical point and after the second point. The obtained flow fields demonstrated two separate supersonic zones on the projectile.

The "critical behavior" of aerodynamic coefficients actually depends on the particular geometry of a boat-tailed projectile. Kuzmin and Babarykin [3] studied 3D flow over a projectile that admits a coalescence of local supersonic zones. In such a case, the interpretation of transonic critical behavior proposed by Budge is not valid. It was suggested in [3] to explain the critical behavior by a shock wave interaction with a supersonic region located downstream. Numerical simulations were performed using a k-ω Shear Stress Transport turbulence model and an assumption of flow symmetry about the pitch plane. The simulations showed that the first minimum in pitching moment coefficient versus M_∞ was indeed associated with the coalescence of local supersonic regions on the lower side of projectile. Meanwhile causes of the second minimum remained unclear.

In the present work, we consider the same projectile as in [3] and perform flow simulations on finer meshes in both a full computational domain enclosing the projectile and a half of the domain located on one side of the symmetry plane. First, we formulate the problem and describe a numerical method. After that we discuss obtained solutions and concentrate on the location of shock waves and supersonic zones on the projectile.

Application of Mathematics in Technical and Natural Sciences
AIP Conf. Proc. 2953, 060005-1–060005-6; https://doi.org/10.1063/5.0177488
Published by AIP Publishing. 978-0-7354-4720-2/$30.00

PROBLEM FORMULATION AND NUMERICAL METHOD

The profile of an axisymmetric projectile under consideration is as follows:

$$\left.\begin{array}{ll} \text{circular-arc nose} & (x-4)^2+(y+7.5)^2=8.5^2 \ \text{ at } \ 0\le x\le 4, \\ \text{horizontal segment} & y=1 \ \text{ at } \ 4\le x\le 6.4, \\ \text{vertical segment} & x=7 \ \text{ at } \ 0\le y\le 0.73, \\ \text{a parabolic arc connecting these segments.} & \end{array}\right\} \qquad (1)$$

The Cartesian coordinates (x,y,z) are dimensional and given in decimeters. A rotation of the profile (1) about the x-axis creates the projectile surface.

For numerical simulation of 3D airflow over the projectile, we use the unsteady Reynolds-averaged Navier-Stokes (URANS) equations [4] with respect to velocity components $U(x,y,z,t)$, $V(x,y,z,t)$, $W(x,y,z,t)$, flow density $\rho(x,y,z,t)$, and static temperature $T(x,y,z,t)$ where t is time. The air is treated as a perfect gas in which the static pressure $p(x,y,z,t)$ is related to density and temperature by the equation of state $p = \rho RT$, where $R = c_p - c_p/\gamma$ is the specific gas constant, c_p=1004.4 J/(kg K) is the specific heat at constant pressure, and $\gamma = 1.4$ is the ratio of specific heats.

The outer boundary of the computational domain is created by a rotation of two circular arcs with endpoints $x=\pm 400$, $y=600$ about the x-axis, see Figure 1. On the inflow part of the boundary, Γ_1, we prescribe the static temperature $T_\infty = 250$ K, angle of attack α and free-stream Mach number $M_\infty < 1$ which determine velocity components $U_\infty = M_\infty a_\infty \cos\alpha$, $V_\infty = M_\infty a_\infty \sin\alpha$, where $a_\infty = (\gamma R T_\infty)^{1/2}$ is the sound speed. The z-component of flow velocity W_∞ vanishes on Γ_1, and free-stream turbulence level is set to 1%.

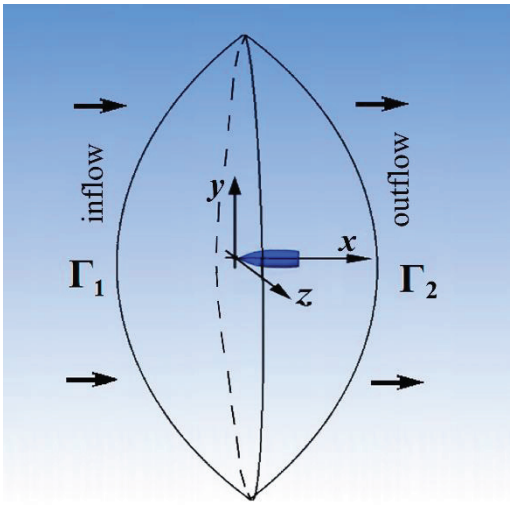

FIGURE 1. A schematic of the computational domain

On the outflow part of boundary, Γ_2, we prescribe the static pressure $p_\infty = 5\times10^4$ N/m^2. The vanishing heat flux and no-slip condition are imposed on the projectile surface. Initial data are either uniform free stream or a nonuniform flow obtained for other values of α and M_∞. The Reynolds number based on the projectile length and M_∞=0.945 is 1.2×10^7.

Solutions of the URANS equations were obtained with ANSYS-15 CFX finite-volume solver, which is based on a high-resolution numerical scheme of second-order accuracy in space and time [5]. For a comparison, a few computations were performed with ANSYS-15 Fluent solver, which confirmed the CFX results. We mainly used a k-ω Shear Stress Transport (SST) turbulence model which is known to reasonably predict boundary layer separations [6]. In addition, several computations were performed using a Detached Eddy Simulation model [7] (see Fig. 4 below).

We employed structured 3D computational meshes, as sketched in Figure 2. A basic mesh was constituted by approximately 18×10^6 hexahedrons and 3.5×10^5 prisms. The non-dimensional thickness y^+ of the first mesh layer on

the projectile was less than 1.2. Apart from the boundary layer, mesh nodes were clustered in vicinities of shock waves. To improve the resolution of shocks, we also performed computations on a refined mesh in a half of the domain as mentioned below. Test computations using global timesteps of 2×10^{-5} s and 4×10^{-5} s yielded undistinguishable solutions; that is why we employed the time-step of 4×10^{-5} s for the study of aerodynamic coefficients behavior at various free-stream Mach numbers. The root-mean-square Courant-Friedrichs-Lewy number (over mesh cells) was about 8.

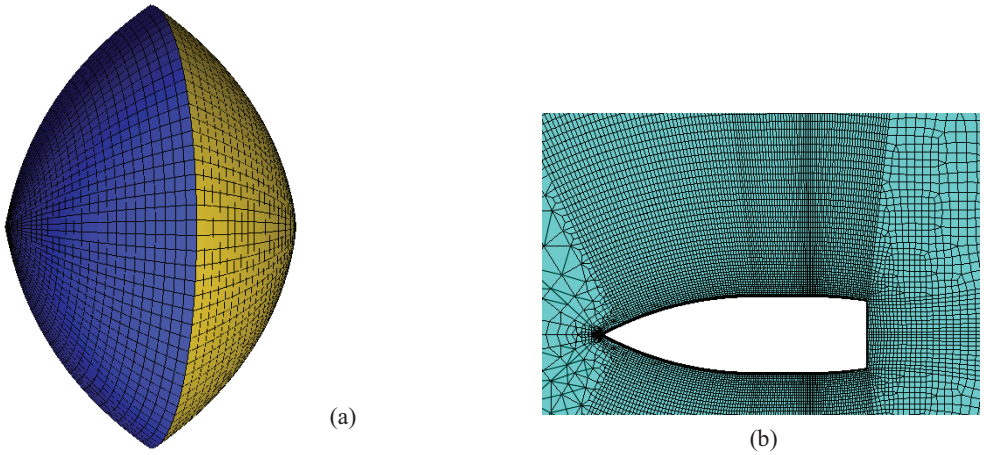

(a) (b)

FIGURE 2. Sketches of the computational mesh: (a) on the outer boundary, (b) near the projectile in the plane (x,y)

RESULTS AND DISCUSSION

Numerical simulations using the free stream as initial data demonstrated a convergence of the mean parameters of turbulent flow to a steady state in less than 0.5 s of physical time. Solutions obtained on the basic computational mesh for several Mach numbers showed that flow fields are symmetric about the pitch plane z=0 (see Figures 3, 4), except for the near wake region which actually did not influence the aerodynamic loads. That is why we performed further computations on a refined mesh of 18.4×10^6 cells generated in the half of computational domain located at z>0, using the symmetry boundary condition on the pitch plane z=0.

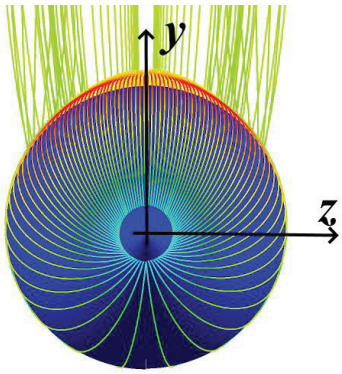

FIGURE 3. A view of streamlines in the positive direction of the x-axis obtained at $M_\infty = 0.946$, $\alpha = 6°$ using k-ω SST turbulence model

The obtained flow fields make it possible to calculate, in particular, aerodynamic forces on the projectile, such as lift L and pitching moment M_{pitch} about the origin. Figure 5 displays the calculated lift coefficient $C_L = 2L/(\rho_\infty U_\infty^2 S)$ and pitching moment coefficient $C_M = 2M_{\text{pitch}}/(\rho_\infty U_\infty^2 S \times 0.7[\text{m}])$ versus M_∞, where $\rho_\infty = p_\infty/(RT_\infty)$, and $S = 0.112594$ m^2 is the area of projectile planform.

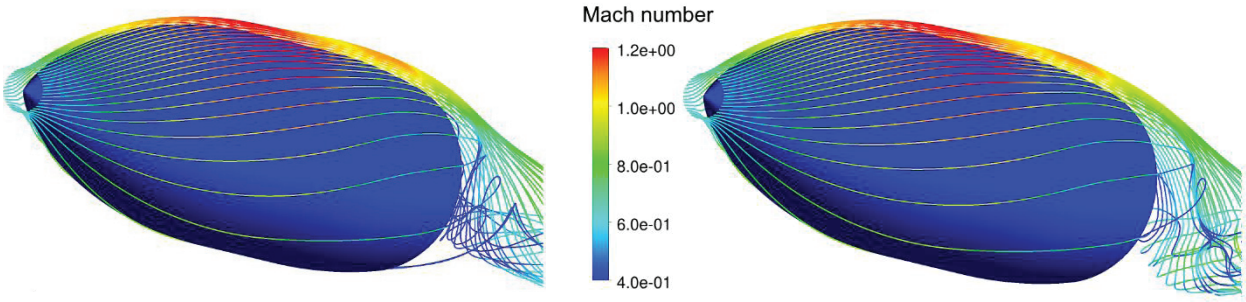

FIGURE 4. Streamlines over the projectile at $M_\infty = 0.946$, $\alpha = 6°$ obtained using k-ω SST turbulence model (left) and Detached Eddy Simulation (right)

An interpretation of the discontinuities in the curves at $M_\infty = 0.940$ is as follows. When $\alpha = 6°$ and $M_\infty < 0.940$, the flow exhibits two separate supersonic regions, see Figure 6. Each region is terminated by a shock wave, behind which the velocity is subsonic. Meanwhile, when M_∞ exceeds 0.940, the local supersonic regions get into a coalescence beneath the projectile, producing an abrupt increase in the supersonic velocities there. As a consequence, the static pressure abruptly decreases on the lower surface of projectile, and this explains the first discontinuity in C_L and C_M . The pointed out phenomenon is similar to the one documented in studies of transonic flow over airfoils [8].

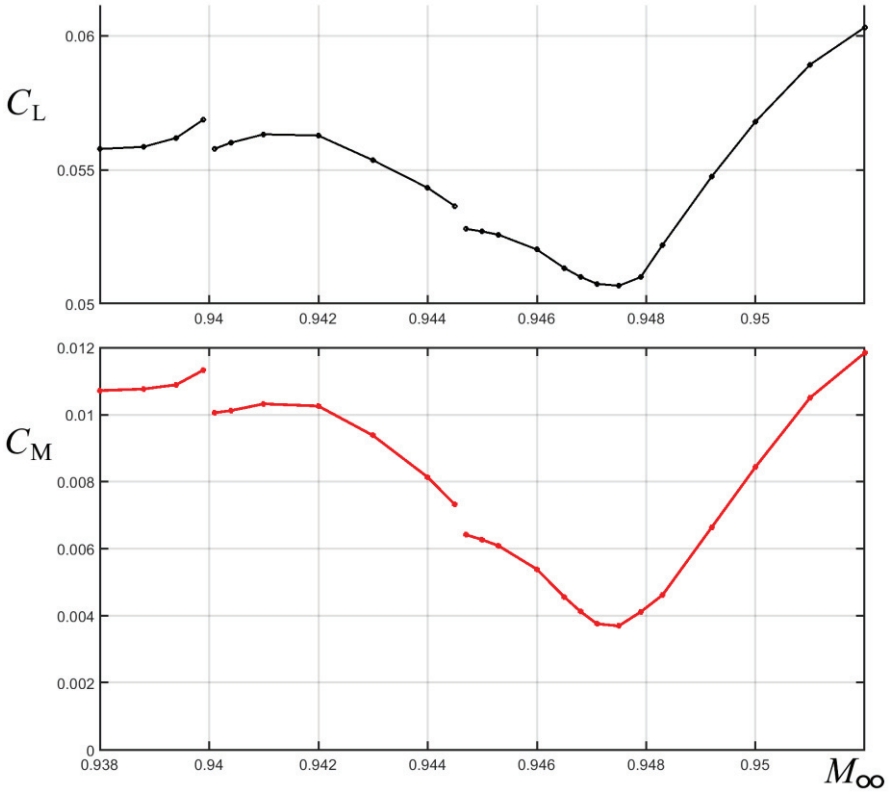

FIGURE 5. The lift and pitching moment coefficients, C_L and C_M, respectively, versus the free-stream Mach number at the angle of attack $\alpha = 6°$

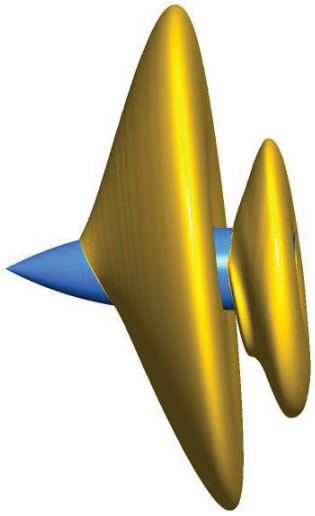

FIGURE 6. Isosurface $M(x,y,z)=1$ in the flow at $M_\infty=0.938$, $\alpha=6°$

At Mach numbers $0.940 < M_\infty \leq 0.9445$ and $\alpha = 6°$, the supersonic regions remain yet separated on the upper surface of the projectile, though they have got into coalescence on the lower surface. Meanwhile, when M_∞ increases to 0.9447, the regions get into a coalescence on the upper surface as well. This causes a second drop in C_L and C_M, see Figure 5. An interpretation of the second drop is as follows. The coalescence of supersonic regions on the upper surface of projectile is accompanied by a shift of the oblique shock SW beneath the projectile towards the base. The supersonic flow in front of SW is adjacent to the convex (parabolic) part of the projectile profile, see Figure 7. Therefore, it expands and speeds up like the Prandtl-Meyer flow over a convex corner. The downstream shift of SW results in an extension of this region beneath the profile where the flow speeds up and pressure drops; as a consequence, the pitching moment and lift drop. This effect persists and causes a further decrease in C_L and C_M when M_∞ increases from 0.9447 to 0.9478.

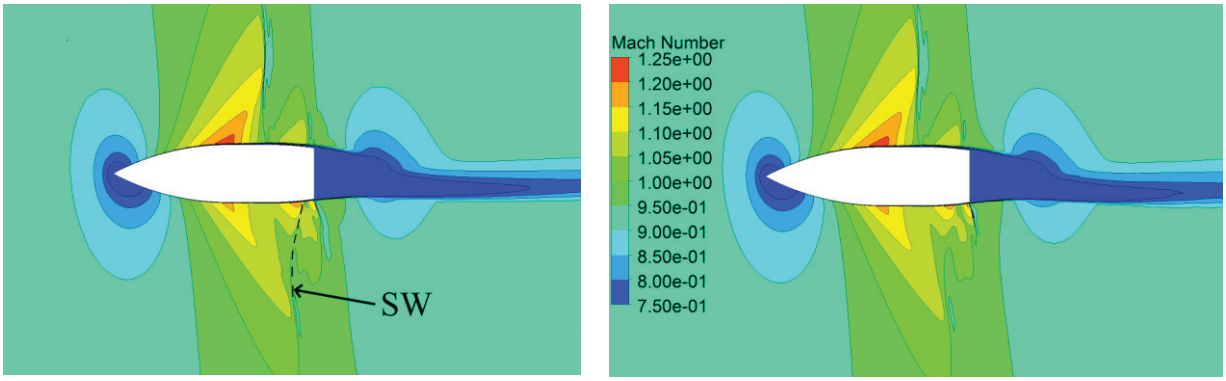

FIGURE 7. Mach number contours in the plane $z=0$ which demonstrate a reflection of shock wave SW from the lower surface of projectile (1) at $M_\infty = 0.9447$, $\alpha = 6°$: CFX solution (left) and Fluent solution (right)

When M_∞ increases from 0.9478 to 0.952, the supersonic region expands above the projectile faster than below it. Therefore, the static pressure decreases on the upper surface of projectile faster than on the lower one, leading to a rise of C_M.

Computations showed that, at the smaller angle $\alpha = 4°$, the behavior of aerodynamic coefficients is similar to that at $\alpha=6°$. As seen from Figure 8, the second discontinuity in C_M is even larger than in the case $\alpha = 4°$. Figure 9 illustrates a considerable decrease of the pressure on the lower surface of projectile near the base with increasing M_∞ from 0.944 to 0.946. As mentioned above, this is caused by a shift of SW towards the base and flow acceleration along the convex part of projectile profile.

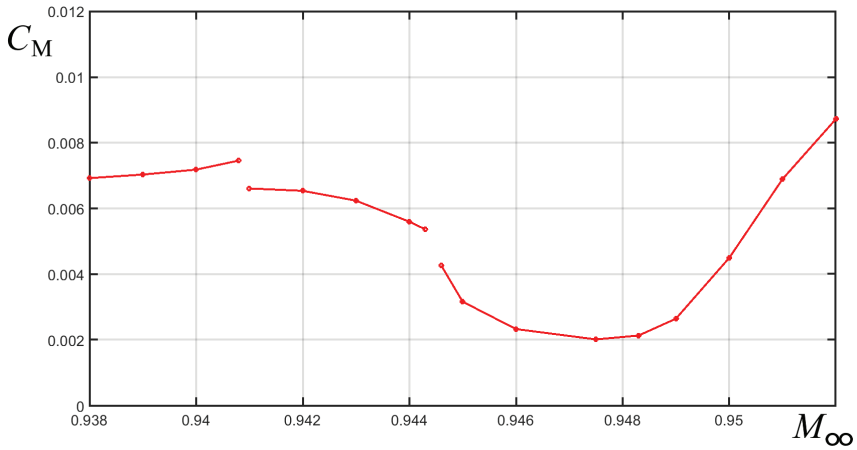

FIGURE 8. The pitching moment coefficient C_M versus the free-stream Mach number at $\alpha = 4°$

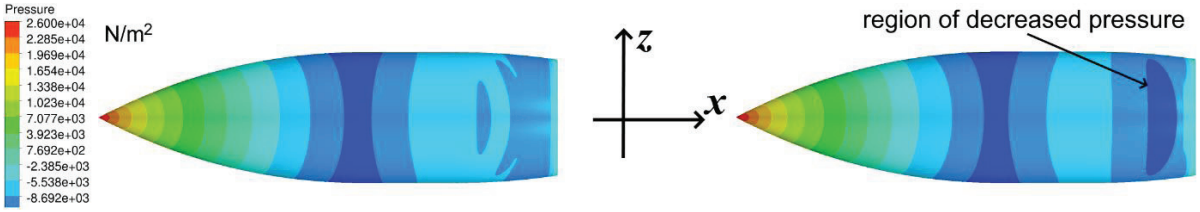

FIGURE 9. The lower surface of projectile: static pressure distributions at $\alpha = 4°$, $M_\infty = 0.844$ (left) and M_∞=0.846 (right)

CONCLUSIONS

The numerical simulation of 3D transonic flow over projectile (1) at the angles of attack $\alpha = 6°$ and $\alpha = 4°$ revealed discontinuities in the aerodynamic coefficients C_L, C_M as functions of the free-stream Mach number M_∞. The first discontinuity occurs due to an abrupt coalescence of local supersonic regions on the lower surface of projectile. The second discontinuity and subsequent drop of C_L, C_M are explained by a coalescence of local supersonic regions on the upper surface and related flow acceleration beneath the projectile along its convex tail. A comparison of results obtained using ANSYS CFX and Fluent solvers showed their good agreement.

ACKNOWLEDGEMENTS

This research was performed using computational resources provided by the Computational Center of St. Petersburg State University (http://cc.spbu.ru). The work was supported by a grant (ID 93935136) from the University.

REFERENCES

1. J. Sahu and C.J. Nietubicz, J. Spacecraft and Rockets **31,** 106–113 (1994).
2. A.M. Budge, Aerodynamic fuze characteristics for trajectory control, Master's thesis, MIT, Cambridge, MA, USA, 1998.
3. A. Kuzmin and K. Babarykin, ARPN J. Engineering and Applied Sciences **13,** 1742–1746 (2018).
4. H. Tennekes and J.L. Lumley, *A First Course in Turbulence* (MIT Press, Cambridge, MA, USA, 1992).
5. ANSYS Fluids - Computational Fluid Dynamics, https://www.ansys.com/products/fluids (2022).
6. F.R. Menter, Int. J. Computational Fluid Dynamics **23**, 305–316 (2009).
7. P. Spalart, Int. J. Heat Fluid Flow **21**, 252–263 (2000).
8. A. Kuzmin, Computers and Fluids **63**, 1–8 (2012).